ERT applied to the study of saltwater intrusion

Author: Pol Garcia Garcia.
Facultat de Física, Universitat de Barcelona, Diagonal 645, 08028 Barcelona, Spain.

Advisor: Perla Piña-Varas and Pilar Queralt Capdevila

Abstract: Sea water intrusion, or saltwater intrusion (SWI) is a common phenomenon in coastal aquifers. With electrical resistivity tomography (ERT) method, a region's subsoil can be characterized, leading to pseudo-section maps that allow to differentiate between freshwater and saltwater cavities. In this study, ERT method was applied in the *Riera de Sant Pol de Mar*, in two different surveys a month apart; which permitted to measure a strong variation between both and track the aquifer's underground evolution. This allowed the observation and analysis of the seawater intrusion phenomenon. If combined with additional methods or information, a better understanding of the diverse processes that occur beneath the aquifer's surface could be achieved.

I. INTRODUCTION

Sea water intrusion, or saltwater intrusion (SWI) is a common phenomenon in coastal aquifers. It consists in the saline water flow from the sea into underground deposits of freshwater, and its impact has direct repercussion on local industries as well as the borderlands' irrigation, given that this event results in aquifers with lower quality freshwater.

The main causes for SWI are found in the over-exploitation of the aquifer, which leads to a dryer underground, permitting seawater to filter into the soil where we should find freshwater; and also in an insufficient input of rainwater to the aquifer, causing the aquifer to dry in a more natural way, but heading to the same consequences. This occurs due to a higher water pressure and higher density for the saline water, which permits seawater to enter inland thanks to the soil porosity. This event is aggravated in dryer aquifers because groundwater has even less pressure than it should, giving a lower opposition to SWI [1].

It was around early 1900s that Willem Badon-Ghyben and Alexander Herzberg made the first physical formulation of this process. This derives to a relation between the freshwater zone thickness below, and above the sea level, resulting in a ratio of 1 to 40 meters of freshwater thickness in the aquifer [2].

While the Ghyben-Herzberg relation uses the different densities of freshwater and seawater for this ratio, there are more techniques that are based on a different physical property. For this project, the technique that has been used is the Electrical Resistivity Tomography (ERT), which is based on the underground resistivity distribution, and provides a sharp contrast between saltwater and freshwater, allowing us to characterize the whole underground region where we take the measure.

By making two separate measures it is possible to keep track of an aquifer's underground evolution, which can be combined with other methods or information for a better understanding of the diverse processes that occur beneath the aquifer's surface. In this case, the rain volume information for the time lapse between the two measurements is a secondary set of data that allows to make further considerations before evaluating the results obtained from the ERT.

The main purpose of this work is to measure this evolution through a month, taking two sets of measurements; and analyse the obtained results to provide a preliminary explanation of the main changes and the different factors that may have been involved in those.

II. EXPERIMENTAL

A. Poisson's equation for heterogeneous media

As previously exposed, the ERT method consists of measuring the electrical resistivity– $\rho, [\rho] = \Omega \cdot \mathrm{m}$ –of the media; which is the physical property that determines a material's opposition to electrical current passage. If Ohm's Law, Null Divergence and electrical field equations are combined, Laplace's equation for homogeneous media is obtained [3]:

$$\nabla \cdot \vec{J} = \frac{1}{\rho} \nabla \cdot \vec{E} = -\frac{1}{\rho} \nabla^2 V = 0 \qquad (1)$$

Being $\vec{J}$ the current density, $\vec{E}$ the electrical field and V the electric potential.

For a non-homogeneous media, it is Poisson's equation which must be used. When applying this equation to the current, I, flow through the ground, and considering the pertinent boundary conditions, the equation for a single source's potential at a distance r, is written [3]:

$$V = \frac{\rho I}{2\pi r} \qquad (2)$$

For a ERT field measure, a minimum of four electrodes is required. Two electrodes, named A and B, are responsible for current injection; while two different electrodes, named M and N, serve as a voltmeter, measuring the electric potential variation between them. Figure 1 shows a standard configuration for these four electrodes.

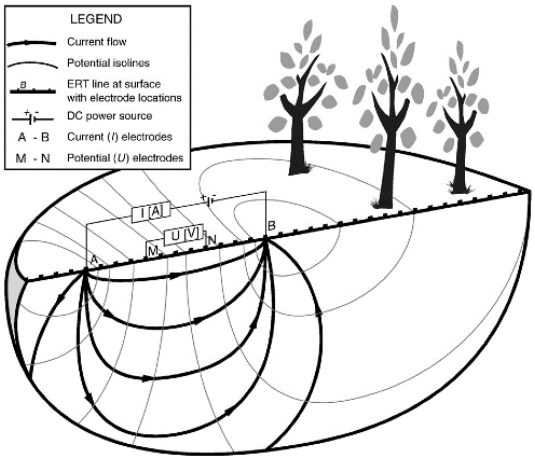

FIG. 1: ERT electrode configuration [4].

If the distance between two given electrodes is noted by XY, where X and Y are the respective electrodes, the electric potential variation between the M and N electrodes is given by [3]:

$$\Delta V_{MN} = \left[\left(\frac{1}{AM} - \frac{1}{MB}\right) - \left(\frac{1}{AN} + \frac{1}{NB}\right)\right] \cdot \frac{\rho I}{2\pi} \qquad (3)$$

This equation can be rearranged to obtain the apparent resistivity, ρ_a, which corresponds to the resistivity, ρ, considering a non-homogeneous media. By defining a geometrical factor K which comprehends the different distances between electrodes, the apparent resistivity of the media can be expressed as [2]:

$$\rho_a = \frac{\Delta V_{MN}}{I} \cdot K \qquad (4)$$

Once determined the expression for the apparent resistivity, all the subsurface area must be studied to obtain the studied area pseudo section, i.e. a map of the subsurface resistivity distribution.

B. Data Acquisition

For the data acquisition, different procedures may be done referred to the electrode configuration used. While its physical position remains the same, the electrodes used for the electrical current injection and the ones used as voltmeter may follow diverse spreads. The ones used in this work are called Wenner-Schlumberger and Dipole-Dipole.

Wenner-Schlumberger arrays use two inner electrodes as M and N, with a b separation between them, while the electrodes A and B are, each, n times b away ($a = nb$) from the M and N electrodes, respectively. This configuration not only covers ascending n values, but also takes higher values for a.

On the other hand, Dipole-Dipole arrays use two pairs of electrodes, serving as injection and voltmeter, separately. Each pair's electrodes are separated a distance a between them, while the AB and MN dipoles are distanced by n times a.

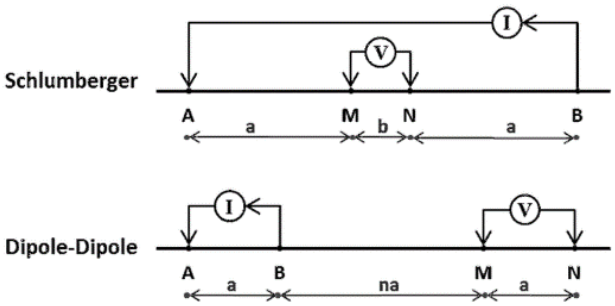

FIG. 2: Wenner-Schlumberger and Dipole-Dipole arrays' diagrams [5].

It is in the data-logger where these different configurations are prepared. Before initiating the measurement process, it is required to select which array must be used. The device will automatically assign to the corresponding electrodes the function they are required for, and will permutate the different assignations until all the desired data is acquired.

C. Inversion

Once acquired all the field data, it is necessary to solve the inverse problem. The inversion's purpose is to simulate the subsurface media composition with an iterative method, getting as a result an underground model that is compatible with the obtained data.

Before the inversion process is done, data must be treated. From the data-logger a .bin file is obtained, including all the electrodes position and resistivity data. The Prosys III software allows to convert this file into a .dat document including only the required information. Prosys III (Iris Instruments) also permits a data filtration to ensure no negative or incoherent values are considered in future stages.

The inversion is then done with the ResIPy inversion and modelling software [6], which also allows to pre-process the data, deleting any point that is considered invalid, such as very high resistivity values that may be caused by an open connection.

For the inversion, each value for the resistivity is considered to be from the mid-point between the injection dipole and the voltmeter dipole. For Wenner-Schlumberger profiles, this mid-point matches the mid-point of each couple. In the case of Dipole-Dipole arrays, depth resolution is provided due to this fact.

While the horizontal position comes directly from the data, the depth resolution obtained is bound to the distance between the injection electrodes' mid-point and the voltmeter electrodes' mid-point, and also to the fraction of current that penetrates between a given depth and the surface.

On the final inversion, a subsurface map will be obtained. This map's display will be a colour gradient map that corresponds to the resistivity calculated value for each point or region.

D. Field Work

The chosen location for this study was the *Riera de Sant Pol de Mar*, located at $41°36'00''N$, $2°37'09''E$, in the *Maresme* zone. Three sets of data were acquired: a short, 142 m, Wenner-Schlumberger (W-S) profile; a long, 284 m, Wenner-Schlumberger profile; and a long, 284 m, Dipole-Dipole (D-D) profile; as shown in FIG. 3. All three of the profiles were perpendicular to the coastline.

Data was acquired specifically for this study, using a Syscal Pro Switch 72 from IRIS Instruments. Despite the three types of array were made, due to the limitation in length of this report, only the results obtained with the Wenner-Schlumberger array are shown. This decision is taken due to Wenner-Schlumberger profile being the only one which was recorded for both long and short profiles.

FIG. 3: ERT study location with the measured profiles.

Two surveys were performed one month apart; the first one on Monday 7th of March and the second one on Wednesday 6th of April. The exact same profiles were acquired in both surveys. Although the first measure was after several days of dry weather without precipitation, the second set of data is preceded by a month with wetter weather and usual rainfall. This climatological factors are expected to be noticed on the results.

Regarding the geology, this zone represents a typical coastal alluvial aquifer, composed by layers of gravels, sands and clays, with granitic basement.

Before collecting the data, the instrumental devices must be prepared. Once selected the area where the measure will take place, it is necessary to install the electrodes; in this case a total of seventy-two; in a straight line, with an equidistant separation. Depending on the profile length that needs to be done, the distance between the electrodes may vary. For this project, the chosen distances were 2 m for a 142 meters short profile and 4 m for a 284 meters, longer profile.

Being the instrumentation properly set, the measure is done automatically by the data-logger, which holds a selection of pre-set configurations depending on the desired type of acquisition.

III. RESULTS AND ANALYSIS

As the processing was made, it has been noticed a 5% maximum of invalid data points, since there were negative values that do not correspond to real measurements. It has also been checked how this misfit points alterate the final inversion, concluding that they have no qualitative effect, for high and low resistivity regions remain on the same place, even if there are light variations on its shape.

For the inversion process, it has been set a maximum of 25 iterations for each model, which have not been needed. The tolerance towards the model misfit was stablished in 0.35, as lower values tend to generate anomalous or abnormal local bodies difficult to interpret. Data fit for the long Wenner-Schlumberger profile, taken on the first day survey, is exposed, as a way of example, in Figure 4.

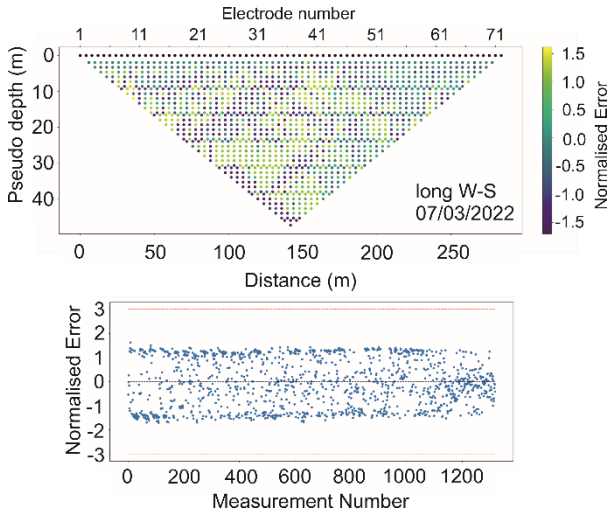

FIG. 4: Wenner-Schlumberger, long profile, data fit for first survey measurement, on March 7th.

Figures 5 and 6 show the resultant inversion models for both surveys, 07.03.2022 and 06.04.2022, respectively.

For each subsurface map, the zero-mark point indicates the higher end of the profile, meaning it is the farther point from the shore. In opposition, the other end (284 m for long profiles and 142 m for the short one) refers to the nearer point to the coastline. It has to be noted that the short profile is located at the centre of the long ones, not at any of its ends.

Observations are made on the Wenner-Schlumberger array for both surveys, since it is the profile which is performed in both long and short profiles. Also, this type of array has a higher resolution, thus making the analysis far more accurate.

On Figure 5, the inversions for W-S array profiles on 07.04.2022 are shown, being this the first set of data. All inversions' colour scales have been stablished from 0.0 to 4.0 to facilitate the comparison between them. Different regions may be spotted, with a distribution of very high and very low resistivity values with no apparent ordination or pattern

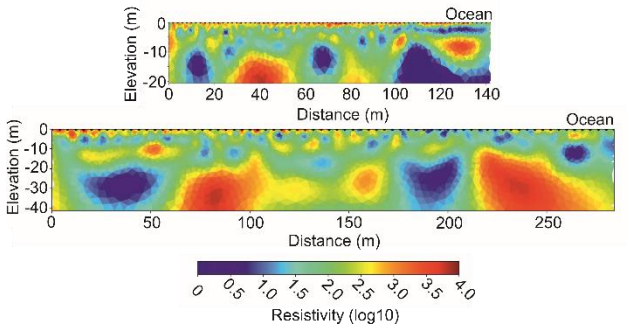

.

FIG. 5: Obtained inversions for the short W-S and long W-S profiles, respectively, on the first survey.

Between the 50 m and 100 m landmark, and from 210 m to the shore, high resistivity regions are found, being the second one wedge-shaped. These bodies present resistivities of the order of $10^3 \Omega \cdot m$ and higher. From 0 m to 50 m, approximately, and within the 175 m to 210 m range, measurements show very low resistivity values, all contained between $1\,\Omega \cdot m$ and $10\,\Omega \cdot m$. In addition, more low-resistivity bodies, of smaller size, are seen at 265 m near the surface, meaning it is very close to the coastline.

On the other hand, figure 6 shows W-S array profiles for the second set of data, corresponding to 06.05.2022. Although the colour scale remains the same that that from the first day, a very smother contrast between regions is appreciated, with a resistivity distribution that doesn't achieve values over $10^3 \Omega \cdot m$, although it has a threshold at $10\,\Omega \cdot m$.

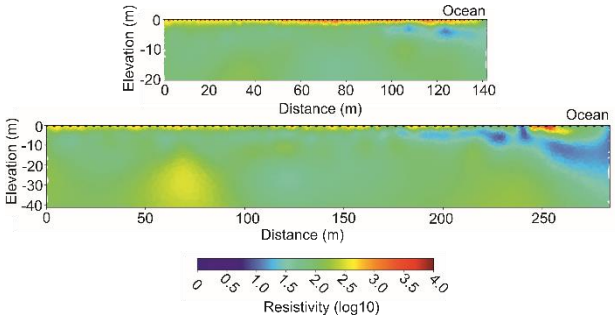

FIG. 6: Obtained inversions for the short W-S and long W-S profiles, respectively, on the second survey.

For this day, it is visible a wide area of higher resistivity, around $10^2 \Omega \cdot m$, extending all over the studied subsoil region. While this fact smoothens all the model, there are still some remarkable traits to notice.

In the western region, for longitudes going from 50 m to 75 m, a higher resistivity body may be spotted, with values over $10^2 \Omega \cdot m$. It may be observed, as well, a tiny region around the 230 m landmark where soil appears to be slightly more resistive than its surroundings.

On the superficial zone near the shore, a thin layer of low resistivity is seen. This low-resistivity body, with values below $10\,\Omega \cdot m$, could correspond to the seawater wedge.

From *Servei Meteorològic de Catalunya (SMC)* there's a constatation on pluviometric data, demonstrating there were several days without rainwater input on the area (given that the data is taken from the *Canet de Mar* meteorologic station) before the first acquisition; while the week before the second survey had been wetter, with abundant rain on Wednesday 30.03.2022. Accumulated rainwater precipitation for the previous 7 days is exposed on Table 1.

TABLE 1: Accumulated precipitation, in $l \cdot m^{-2}$ over the previous seven days on *Canet de Mar* meteorologic station. [Data provided by *SMC* [7].]

Date	**Accumulated precipitation ($l \cdot m^{-2}$)**
07.03.2022	0.0
06.04.2022	32.5

Apart from the inverse problem, the difference between the first and the second data sets has been calculated for each array. It was also calculated the quotient between the measures [8]. Finally, an inversion was made for the resulting data, obtaining models for the subsurface distribution that ought to be if it were to be measured that difference.

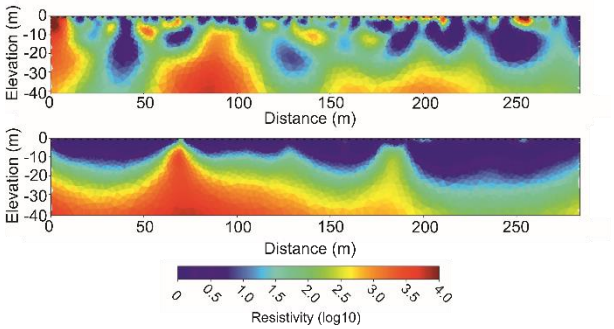

FIG. 7: Obtained inversions for the long W-S data difference and quotient, respectively.

This results have to be taken with caution and cannot be directly compared with the other models obtained, for these models do not correspond to any real data or soil configuration. However, they might be useful towards interpretating the occurred variation. Figure 7 shows both the gradient and the quotient between measurements for the W-S long profile.

The gradient model minimizes the systematic error related to the acquisition itself. Meanwhile, the quotient model emphasizes the differences between the models from both surveys. More work is needed in this sense to fully understand the implications of the gradient and quotient models.

IV. DISCUSSION

By comparing the two surveys, it is clearly seen there has been an evolution on the underground resistivity. While the soil composition; referring to the clays, sands and silicates that compound it; must be the same, seawater or freshwater presence may be responsible for the different data recorded.

Table 2 shows the main ranges for distinct types of water and soil resistivity. This information may suggest not only a stony body located in the 50 m to 75 m range, below the twenty-meter level; but also a swampy soil region on the surface for longitudes going from 180 m to 240 m, which can be appreciated on the second day inversions. This guess is coherent with the observed environment on the second day, where the section before (i.e. lower distances, following the chosen criteria) the train bridge was muddy.

TABLE 2: Usual values for resistivity [9], [10].

Water Type	Resistivity	Soil Type	Resistivity
Precipitation	30-1000 Ωm	Stony ground	1500-3000 Ωm
Surface water	10-100 Ωm	Siliceous sand	200-300 Ωm
Groundwater	0.2-8.8 Ωm	Chalky soil	100-300 Ωm
Seawater	0.2 Ωm	Swampy soil	1-30 Ωm

More interesting than that, is approaching the situation from the inverse point of view. While the second data set was taken a month after the first, it shows a wet subsoil, with a wide area of resistivity values of the 10^2 order. Since the soil composition cannot change, the values obtained from the first survey shall belong to an identical, but dryer, ground composition.

This means, in first place, that the soil has a high permeability that allows freshwater to filtrate to the soil.

In second instance, this implies that in absence of groundwater, seawater intrudes inland, allocating in punctual cavities that are observable on the first survey's inversions.

After the rain period (06.04.2022; Fig.6) the resistivity model shows smoother variations. However, it is in this model where the shallow, conductive body close to the coastline can be appreciated more clearly.

V. CONCLUSIONS

After having made two surveys for the same aquifer, separated by a whole month, visible results were expected to appear when doing the inversions. Furthermore, the wetter weather days before the second field trip was of much help to accentuate the subsoil evolution after a freshwater input. This way, after analysing the results and approaching it as a reverse process, seawater intrusion phenomenon could be clearly observed.

Besides, the high contrast between the two sets of data permits a further analysis of the subsoil composition, if wanted, given the wide range of data obtained along both surveys. This would grant a major understanding of the whole phenomena, and would allow to make less assumptions on the underground configuration.

Nevertheless, given the main purpose and focus of this work, both the realization and the results are satisfactory, not only for the vast range of possibilities it offers, but for the knowledge acquired in the realization itself, which has been very fulfilling.

Acknowledgments

In first place, I would like to thank Perla Piña, my advisor, for all the time and patience invested into this project, for not giving up; Pilar Queralt, for this wonderful opportunity and her vast knowledge in geophysics; and David Garcia, for his tireless dedication. I would also like to thank Gemma, Fabian and José Tur for their support, as well as my friends and colleagues. Finally, a special and warm thank to Gemma, for her energy and confidence.

[1] L. d. V. L. L. L. M.-P. F. B. H. L. L. V. R. N. F. A. P. S. F. M. M. M. D.-F. M. P. T. G. J. L. P. P. O. B. P. Q. A. M. J. G.-O. A. Folch, «Combining fiber optic DTS, cross-hole ERT and time-lapse induction logging to characterize and monitor a coastal aquifer,» *Journal of Hydrology*, vol. 588, 2020.

[2] L. Chartier, *Coastal Aquifer Characterization using Electrical methods*, Treballs Finals de Grau de Física, Facultat de Física, Universitat de Barcelona, 2019.

[3] P. Queralt, «Exploració Geofísica,» 2021.

[4] S. M. R. A. H. W. N. a. M. v. d. M. de Jong, «Monitoring Soil Moisture Dynamics Using Electrical Resistivity Tomography under Homogeneous Field Conditions,» *Sensors*, vol. 20, nº 18: 5313, 2020.

[5] F. Garofalo, *Physically constrained joint inversion of seismic and electrical data for near-surface application*, Politecnico di Torino, 2014.

[6] S. S. J. B. P. M. A. B. Guillaume Blanchy, *ResIPy, an intuitive open source software for complex geoelectrical inversion/modeling*, vol. 137, 2020.

[7] «Servei Meteorològic de Catalunya,» [En línea]. Available: https://www.meteo.cat/wpweb/serveis/cataleg-de-serveis/dades-meteorologiques/#xema.

[8] D. Bosch, *Tomografia elèctrica a escala de laboratori: investigació del sistema roca-salmorra-CO2*, Universitat de Barcelona, 2015.

[9] R. &. T. E. Saad, «Groundwater Detection in Alluvium Using 2-D Electrical Resistivity Tomography (ERT),» *Electronic Journal of Geotechnical Engineering*, nº 17, 2012.

[10] «Engineering ToolBox, Soil Resistivity,» 2013. [En línea]. Available: https://www.engineeringtoolbox.com/soil-resistivity-d_1865.html.